Instrumentation for the Investigation of Pitch Bearing Design and Reliability

Jon Keller,[1] Jesse Graeter,[2] Jason Roadman,[1] and Miles Skinner[1]

1 National Renewable Energy Laboratory
2 ONYX InSight

NREL is a national laboratory of the U.S. Department of Energy
Office of Energy Efficiency & Renewable Energy
Operated by the Alliance for Sustainable Energy, LLC

This report is available at no cost from the National Renewable Energy Laboratory (NREL) at www.nrel.gov/publications.

Contract No. DE-AC36-08GO28308

Technical Report
NREL/TP-5000-87719
April 2024

Instrumentation for the Investigation of Pitch Bearing Design and Reliability

Jon Keller,[1] Jesse Graeter,[2] Jason Roadman,[1] and Miles Skinner[1]

1 National Renewable Energy Laboratory
2 ONYX InSight

Suggested Citation
Keller, Jon, Jesse Graeter, Jason Roadman, and Miles Skinner. 2024. *Instrumentation for the Investigation of Pitch Bearing Design and Reliability*. Golden, CO: National Renewable Energy Laboratory. NREL/TP-5000-87719.
https://www.nrel.gov/docs/fy24osti/87719.pdf.

NREL is a national laboratory of the U.S. Department of Energy
Office of Energy Efficiency & Renewable Energy
Operated by the Alliance for Sustainable Energy, LLC

This report is available at no cost from the National Renewable Energy Laboratory (NREL) at www.nrel.gov/publications.

Contract No. DE-AC36-08GO28308

Technical Report
NREL/TP-5000-87719
April 2024

National Renewable Energy Laboratory
15013 Denver West Parkway
Golden, CO 80401
303-275-3000 • www.nrel.gov

NOTICE

This work was authored in part by the National Renewable Energy Laboratory, operated by Alliance for Sustainable Energy, LLC, for the U.S. Department of Energy (DOE) under Contract No. DE-AC36-08GO28308. Funding provided by the U.S. Department of Energy Office of Energy Efficiency and Renewable Energy Wind Energy Technologies Office. The views expressed herein do not necessarily represent the views of the DOE or the U.S. Government.

This report is available at no cost from the National Renewable Energy Laboratory (NREL) at www.nrel.gov/publications.

U.S. Department of Energy (DOE) reports produced after 1991 and a growing number of pre-1991 documents are available free via www.OSTI.gov.

Cover Photos by Dennis Schroeder: (clockwise, left to right) NREL 51934, NREL 45897, NREL 42160, NREL 45891, NREL 48097, NREL 46526.

NREL prints on paper that contains recycled content.

Acknowledgments

The authors would like to thank Mark Iverson and Simon Thao of the National Renewable Energy Laboratory and Adam Cameron and William McConnell of ONYX Insight for their efforts during the installation of the instrumentation.

This report is available at no cost from the National Renewable Energy Laboratory at www.nrel.gov/publications.

List of Acronyms

DOE	U.S. Department of Energy
EDAS	EtherCAT data acquisition system
GE	General Electric
Hz	hertz
m	meter
mm	millimeter
MW	megawatt
m/s	meters per second
NREL	National Renewable Energy Laboratory
rpm	revolutions per minute
s	second(s)
V	volt

This report is available at no cost from the National Renewable Energy Laboratory at www.nrel.gov/publications.

Table of Contents

This report is available at no cost from the National Renewable Energy Laboratory at www.nrel.gov/publications.

List of Figures

List of Tables

This report is available at no cost from the National Renewable Energy Laboratory at www.nrel.gov/publications.

1 Introduction

Average annual operations and maintenance costs have decreased in newer land-based wind power plants in the United States (Wiser et al. 2023). However, total operational expenditures are an important contributor to the overall cost of wind energy at an average of $44 per kilowatt per year with somewhat less than half of that associated with wind turbine operations and maintenance (Wiser, Bolinger, and Lantz 2019). Improving wind turbine component reliability continues to be a priority for the wind energy industry, as more reliable components and better operations and maintenance strategies have the potential to reduce the levelized cost of energy by 10% or more for land-based wind plants (Wiser, Bolinger, and Lantz 2019; Stehly, Beiter, and Duffy 2020) or even more for fixed-bottom, offshore wind plants (Stehly, Beiter, and Duffy 2020).

Recently, there has been increased interest in the reliability of pitch systems (see Walgern et al. 2023) and pitch bearings (Dvorak 2016; Shapiro 2017; Dhanola and Garg 2020; Keller et al. 2021; Doll 2022). Pitch bearings, shown in Figure 1, are used in wind turbines to connect the blade root to the hub. They support simultaneous radial, axial, and overturning moment loads while allowing relative rotation of the blade with respect to the hub. Design requirements for pitch bearings are specified in the International Electrotechnical Commission 61400-1 wind turbine design standard. Additionally, the National Renewable Energy Laboratory (NREL) published a pitch and yaw bearing design guide that summarized the design criteria, calculation methods, and other applicable standards recommended for use in analyzing the performance and life of these bearings (Harris, Rumbarger, and Butterfield 2009). The guide is still widely used today, with a recent example of assessing a typical bearing in use on a 1.5-megawatt (MW) wind turbine (Keller and Guo 2022).

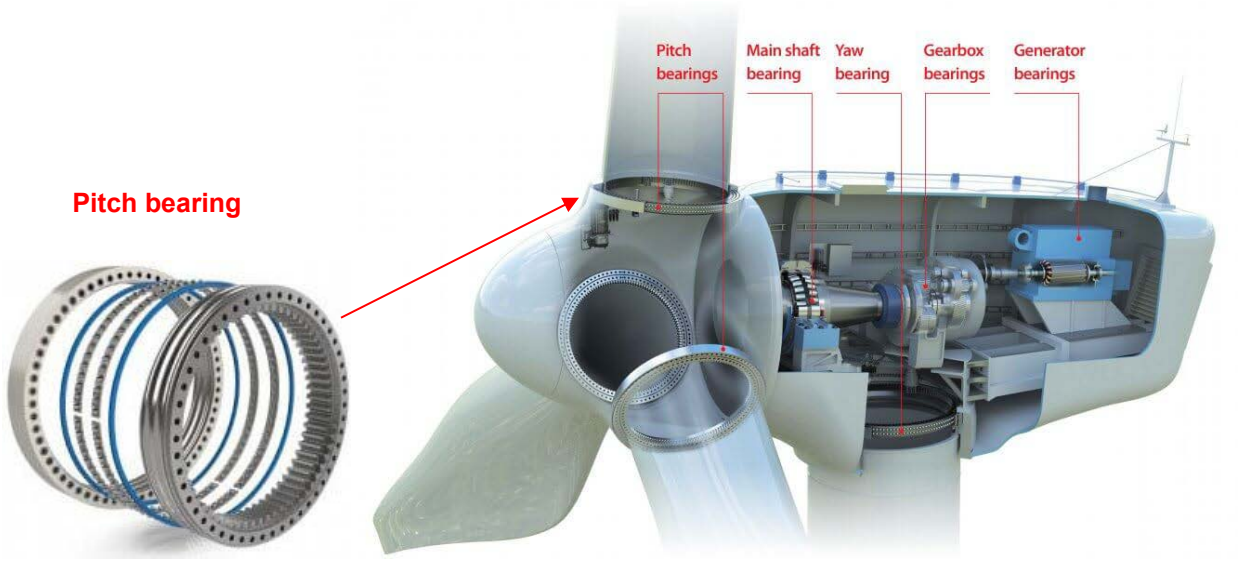

Figure 1. Wind turbine pitch bearing (left) and nacelle (right). ***Image from Bayles (2020)***

Some pitch bearings have a projected 12% failure rate in 20 years (Hornemann 2019). Although comparable information in the literature for existing offshore wind power plants is sparse, it indicates that pitch system failure rates are more than 2 times higher for offshore than land-based wind power plants (Dao, Kazemtabrizi, and Crabtree 2019). These bearings are usually grease-

This report is available at no cost from the National Renewable Energy Laboratory at www.nrel.gov/publications.

lubricated, operate in boundary lubrication conditions because of their oscillating movements, are relatively susceptible to contamination, and can experience extended periods of little to no rotation (Shapiro 2017). As rotor diameters continue to increase for land-based and offshore wind turbines, pitch bearings are becoming even larger in diameter, which can make them vulnerable to deflections and stress concentrations. With the introduction of advanced controllers, the pitch travel characteristics of these bearings have changed. For these reasons, there is an increased need to more accurately study pitch bearing deformations, misalignment, load distributions, and contact stresses (Keller et al. 2021; Keller and Guo 2022).

Significant work has been done to investigate the fatigue lives and wear characteristics of pitch bearings on ground-based test rigs (Handreck et al. 2015; Becker et al. 2017; Grebe et al. 2018; He et al. 2018; Liu et al. 2018; Schwack, Prigge, and Poll 2018; Fischer and Mönnig 2019; Schwack et al. 2020, 2021; Song and Karikari-Boateng 2021; Bartschat, Behnke, and Stammler 2023; Becker et al. 2023; Behnke and Schleich 2023; Graßmann, Schleich, and Stammler 2023; de la Presilla et al. 2023). NREL has also recently begun a research program related to studying pitch bearing reliability, as its importance grows for wind turbines. The purpose of this report is to describe instrumentation that was recently installed on a 1.5-MW wind turbine at NREL's Flatirons Campus and provide an example dataset. To the authors' knowledge, this will be the first publicly available pitch bearing data collection campaign on an operational wind turbine.

This report is available at no cost from the National Renewable Energy Laboratory at www.nrel.gov/publications.

2 Wind Turbine and Pitch Bearing

The U.S. Department of Energy (DOE) installed a General Electric (GE) 1.5-MW wind turbine at NREL's Flatirons Campus over the winter of 2008–2009. This turbine, hereafter referred to as the DOE 1.5, is an integral part of several research initiatives for the DOE Wind Energy Technologies Office and other industry research initiatives.

2.1 Wind Turbine and Instrumentation

The DOE 1.5 is built on the platform of the GE 1.5 SLE commercial wind turbine model but was installed in a nonstandard configuration. Important for this project and others is the fact that the DOE 1.5 is equipped with an ESS Mk 6 controller. Relevant properties of the DOE 1.5 turbine are listed in Table 1.

Table 1. DOE 1.5 Wind Turbine Properties

Parameter	Value	Units[a]
Rated power	1.5	MW
Number of blades	3	-
Hub height	80	m
Nominal rotor diameter	77	m
Rated rotor speed	18.3	rpm
Cut-in wind speed	3	m/s
Cut-out wind speed	25	m/s

[a] m = meter, m/s = meter per second, rpm = revolutions per minute

A series of tests were previously conducted to characterize the properties and performance of the DOE 1.5, including mechanical loads per International Electrotechnical Commission 61400-11 in March 2011 (Santos and van Dam 2015). The test program included specially installed instrumentation throughout the turbine and on a meteorological tower in front of it. Routine measurements acquired on the meteorological tower are air temperature, pressure, humidity, and wind speed and direction at several heights. For the wind turbine, blade pitch angles; rotor azimuth; rotor and generator speed; main shaft, tower, and blade loads; generator torque and power; nacelle yaw; wind speed and direction; and several supervisory control and data acquisition channels are typically recorded.

2.2 Pitch Bearing and Instrumentation

Several suppliers provide pitch bearings for the GE 1.5 wind turbine platform; however, the pitch bearings installed in the DOE 1.5 turbine were supplied by Kaydon with part number 16230001. As illustrated in Figure 2, the pitch bearings (Kaydon DT series slewing bearings) comprise two rings to form the outer and inner raceways with a complement of balls. The ball-groove contact provides two distinct thrust load paths for each ball. This bearing has two rows, thus often called an "eight-point" contact ball bearing. The bearing rings have mounting holes uniformly distributed around the circumference of each ring oriented parallel to the axis of rotation that allow the bearing to be bolted directly to the hub—onto the outer ring—and blade—onto the

This report is available at no cost from the National Renewable Energy Laboratory at www.nrel.gov/publications.

inner ring. The outer ring (OR) of this pitch bearing is stationary, whereas the inner ring (IR) is rotated by an electric motor driving the interior spur gear teeth.

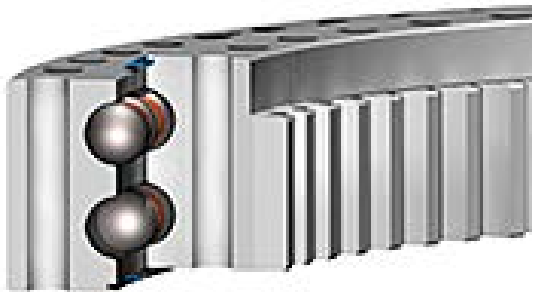

Figure 2. Eight-point contact pitch bearing. ***Image from Kaydon*** **(n.d.)**

The description of the reference bearing in Table 2 is generally representative of the bearings currently in the market.

Table 2. Reference Pitch Bearing Properties

Parameter	Symbol	Value	Units[a]
Pitch diameter	D_{pw}	1,900	mm
Ball diameter	D_w	34.9	mm
Groove conformity (inner and outer raceways)	f	0.53	-
Number of rows	i	2	-
Number of rolling elements (per row)	Z	156	-
Nominal contact angle	α	50	°

[a] ° = degrees, mm = millimeter

The pitch bearing instrumentation package was jointly developed by NREL and ONYX Insight. It is like the instrumentation in many ground-based test rig experiments, but because of channel limitations in the rotating rotor hub there are fewer sensors. Figure 3 shows an overview of the pitch bearing instrumentation package when the blade is at a pitch angle of 0°. The instrumentation comprises:

- Ten strain gages bonded to the stationary OR
- Two strain gages bonded to the rotating IR
- A reference strain gage on the interior of the hub casting
- Four laser displacement sensors targeting the end faces of the IR gear teeth
- A total of two resistance temperature detectors on the OR and IR
- A reference resistance temperature detector on the interior of the hub casting.

We installed all of the sensors on the pitch bearing of blade 1 of the wind turbine *in situ*. Thus, the reference condition for the strain gages and displacement sensors is arbitrary, as the bearing

This report is available at no cost from the National Renewable Energy Laboratory at www.nrel.gov/publications.

is already loaded by the blade weight. Details of the sensors and sensor installations are provided in the following sections and in Appendix A.

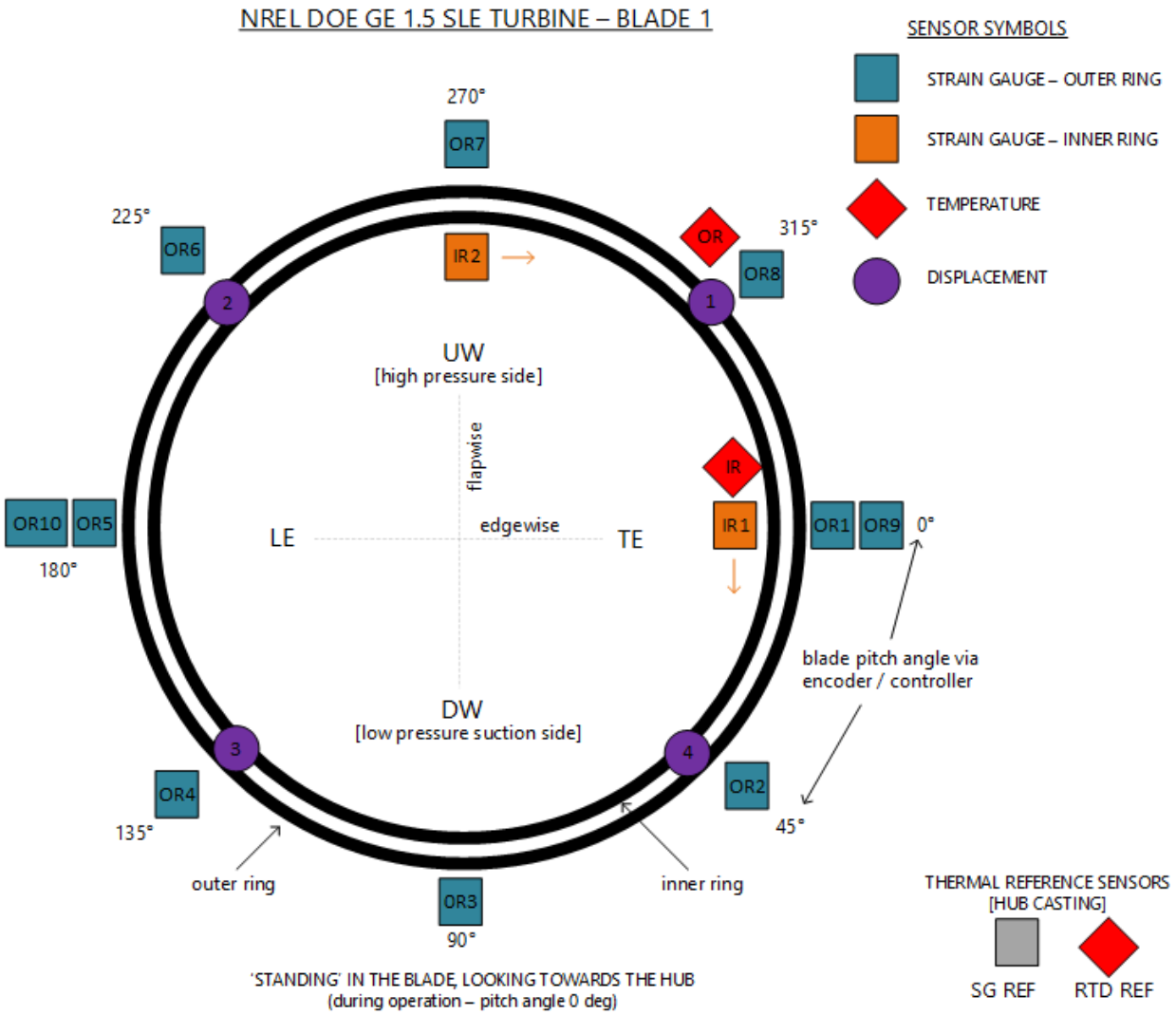

Figure 3. Overview of pitch bearing instrumentation.

DW = downwind, LE = leading edge, REF = reference, RTD = resistance temperature detector; SG = strain gauge, TE = trailing edge, UW = upwind

2.2.1 Strain Gages

All strain gages are type CEA-06-250UWA-350, with a self-temperature compensation designation to match the thermal expansion behavior of steel. They were bonded with AE-10 to a sanded and cleaned surface on either the pitch bearing or hub casting. They are all wired in a quarter-bridge configuration and are recorded as the ratio of bridge output to supply voltage in units of volts per unit volt (V/V). The gages were bonded with AE-10 to the pitch bearing in warm, daytime ambient conditions of approximately 10 to 20° Celsius (°C) and kept near these temperatures while curing overnight using heating pads. The gage factor and thermal output coefficients are given in Table 3.

This report is available at no cost from the National Renewable Energy Laboratory at www.nrel.gov/publications.

Table 3. Strain Gage Properties

Parameter	Symbol	Value	Units[a]
Gage factor	F_G	2.070±0.5%	-
Temperature coefficient of the gage factor		1.5	%/100°C
Thermal output coefficients	A_0	-7.85×10^{1}	με
	A_1	5.02×10^{0}	με/°C
	A_2	-8.20×10^{-2}	με/(°C)^2
	A_3	3.60×10^{-4}	με/(°C)^3
	A_4	-3.54×10^{-7}	με/(°C)^4

[a] °C = degrees Celsius, με = microstrain

The OR trailing edge strain gages are shown in Figure 4 while the OR leading-edge strain gages are shown in Figure 5. All the gages were installed in an orientation with the axis of sensitivity along the pitch bearing circumference, except for a single gage in an axial orientation, as shown in Figure 5. The exact locations of the strain gages from the edges of the pitch bearing rings and from each other are detailed in Appendix A.

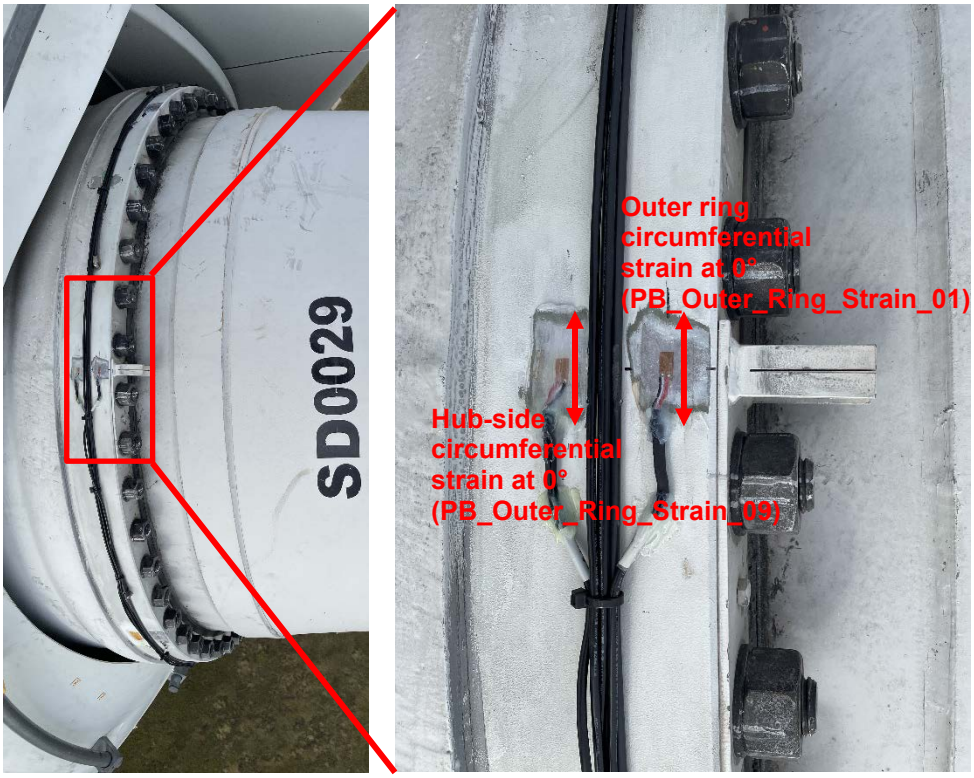

Figure 4. Overview (left) and close-up (right) of outer ring trailing edge strain gages. ***Photos by Jesse Graeter, ONYX Insight, NREL 85947 and 85942***

This report is available at no cost from the National Renewable Energy Laboratory at www.nrel.gov/publications.

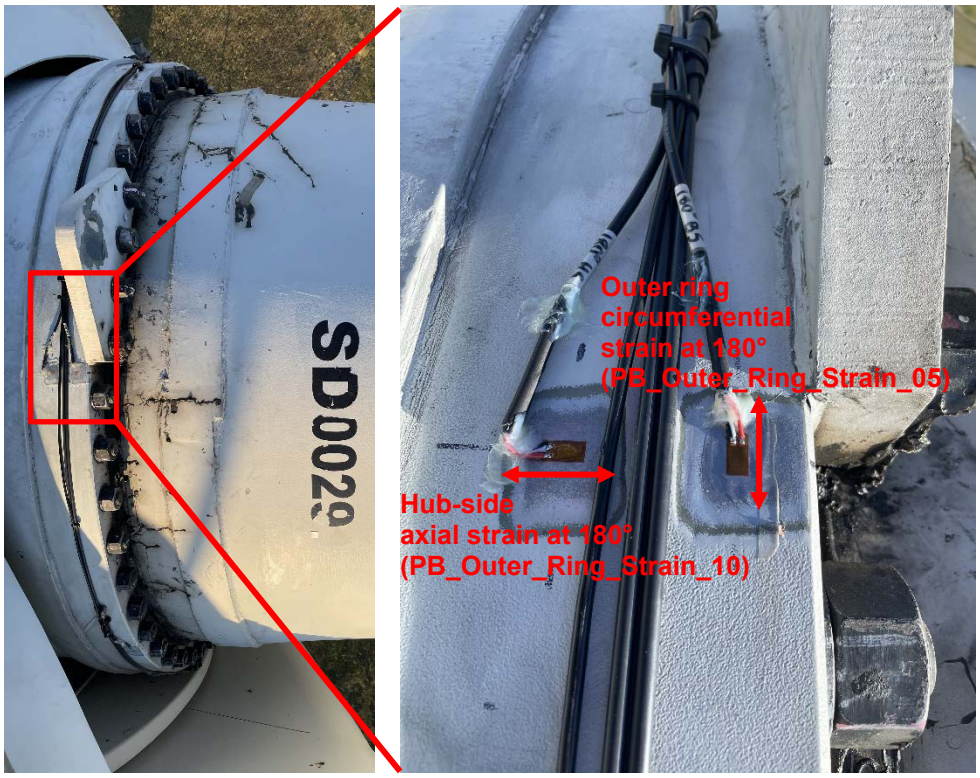

Figure 5. Overview (left) and close-up (right) of outer ring leading edge strain gages. ***Photos by Jesse Graeter, ONYX Insight, NREL 85944 and 85948***

The IR strain gages are shown in Figure 6. The reference strain gage and the reference resistance temperature detector installed on the interior of the hub casting are shown in Figure 7. These sensors are located near the hub entry hatch. The exact locations of the strain gages from the edges of the pitch bearing ring are detailed in Appendix A.

Figure 6. Inner ring strain gages. ***Photo by Jesse Graeter, ONYX Insight, NREL 85940***

This report is available at no cost from the National Renewable Energy Laboratory at www.nrel.gov/publications.

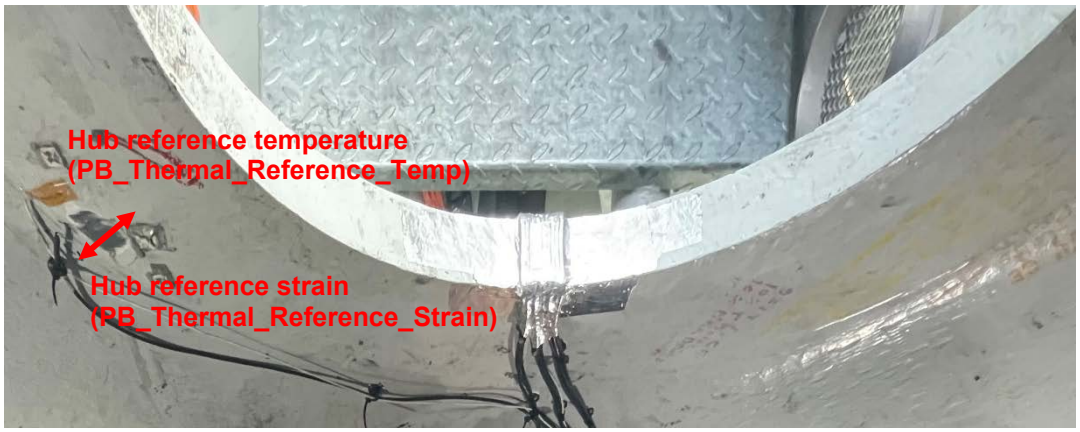

Figure 7. Hub casting reference strain gage and temperature. ***Photo by Jesse Graeter, ONYX Insight, NREL 85946***

2.2.2 Displacement Sensors

We used four optoNCDT ILD1220-10 laser displacement sensors to measure the axial displacement in millimeters of the pitch bearing IR with respect to the hub casting and OR. The sensors are equally spaced around the bearing circumference, as shown in Figure 3, and on brackets attached to the hub casting. Because of clearances, the sensors could not be pointed toward the pitch bearing IR as desired. Instead, they are pointed toward the pitch bearing gear teeth as shown in Figure 8. We placed the sensors such that they are nominally at the midpoint of their measurement range of 20 to 30 mm; however, as the blade pitches in operation, the sensors can occasionally be pointing at the gap between the gear teeth. In this situation, they record either their "zero" value of 20 mm or their full-scale value of 30 mm. The true relative displacement between the bearing rings must be determined by subtracting out each sensor's particular offset, which is best determined from resting conditions.

Figure 8. Relative axial displacement. ***Photo by Jesse Graeter, ONYX Insight, NREL 85943***

This report is available at no cost from the National Renewable Energy Laboratory at www.nrel.gov/publications.

2.2.3 Resistance Temperature Detectors

We used three surface-mount SSP-RTD-PT100-180-MP resistance temperature detectors to measure the temperatures in degrees Celsius of the pitch bearing IR and OR, and the interior of the hub casting as a thermal reference. The resistance temperature detector on the OR, as well as a nearby strain gage are shown in Figure 9.

Figure 9. Outer ring temperature and circumferential strain at 315°. ***Photo by Jesse Graeter, ONYX Insight, NREL 85945***

2.3 Data Acquisition System

A National Instruments EtherCAT chassis is located in the wind turbine hub. The individual sensors are connected to it and the output is converted to digital signals, which are then time synchronized with the other turbine and meteorological system measurements. The data acquisition rates are the "slow" collection rate of 1 hertz (Hz) and the "fast" collection rate of 50 Hz. Slow data are collected for 24-hour periods, whereas fast data are collected for 10-minute periods. All channels are typically recorded in the slow data stream; however, sensors may or may not be collected in the fast data stream, depending on the signal characteristics or other data analysis purposes. The pitch bearing instrumentation is recorded in both data streams. The channel lists and recording rates can also be, and often are, reconfigured to accommodate other projects.

This report is available at no cost from the National Renewable Energy Laboratory at www.nrel.gov/publications.

3 Example Results

An example dataset is examined in this section. Beginning at approximately 8:30 a.m. on October 17, 2023, the wind turbine was in a "slow roll" condition (i.e., rotating at a very low rotor speed). As shown in Figure 10, it began to start up by pitching the blades after approximately 30 seconds (s), which then began to increase the rotor speed. After approximately 180 s, the turbine began generating power. As the wind speed further increased to a range of 8 to 10 m/s, the turbine power increased and reached just over 800 kilowatts while at rated rotor speed. During this period, the air temperature recorded by the meteorological tower at the turbine hub height and the pitch bearing temperatures were all relatively constant from 19 to 20°C.

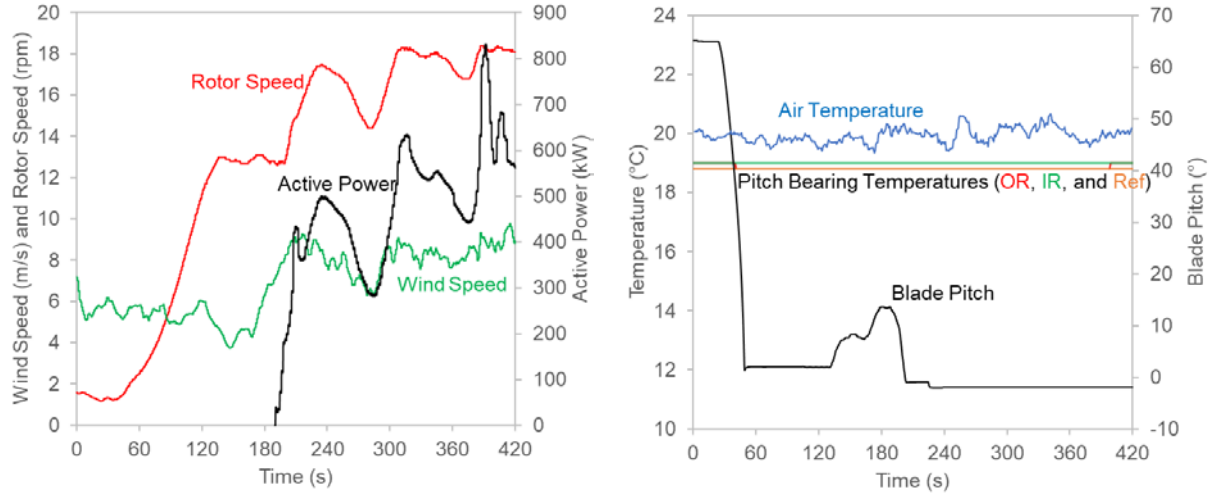

Figure 10. Wind turbine operating parameters (left) and temperature and blade pitch (right)

3.1 Strain

In Figure 11, we examine the example pitch bearing OR strain responses at the trailing- and leading-edge locations in comparison to the reference strain response in units of V/V.

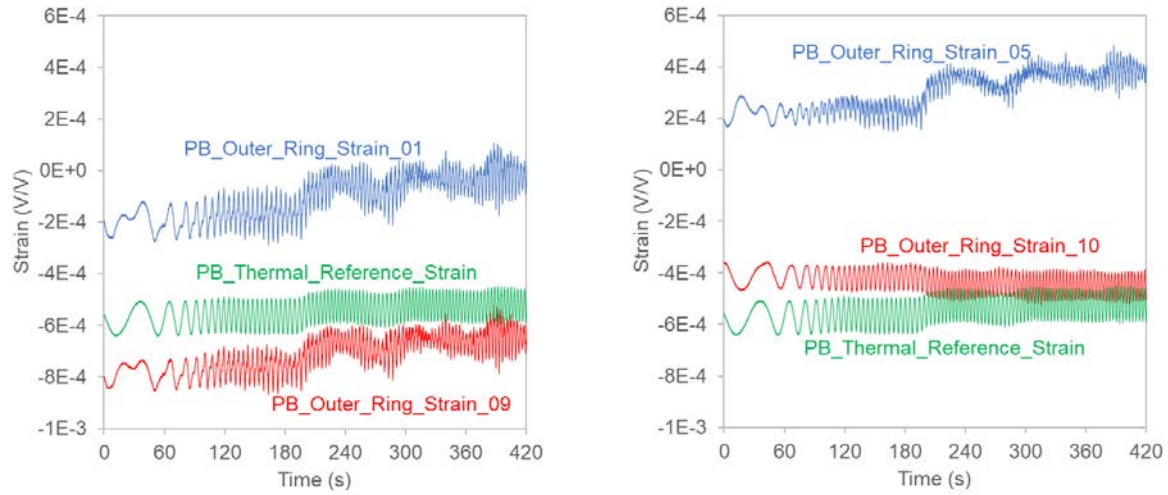

Figure 11. Outer ring trailing edge (left) and leading edge (right) strain in V/V over time

This report is available at no cost from the National Renewable Energy Laboratory at www.nrel.gov/publications.

The measured bridge responses are not balanced, so each contains a natural offset in V/V that is primarily a reflection of small differences in the bridge arm resistances and lead-wire resistance. However, all the strain responses are similar in peak-to-peak magnitude, although the reference strain is the most consistent at approximately 0.20 millivolts per unit volt. Although the reference strain was intended to be in a low-strain environment in the hub casting, it clearly measures changes in strain and load similar to the gages located on the pitch bearing itself.

As part of converting the quarter-bridge strain responses from units of V/V to units of strain, the change in the gage factor with temperature and the change in the strain with temperature should be considered. For the chosen CEA-type strain gages, the change in the gage factor is only 1.5% per 100°C. Thus, over the expected range of temperatures in this application and certainly for this dataset recorded at a constant 19°C, this effect is very small and therefore ignored here. As described earlier, we installed the strain gages on the pitch bearing *in situ* and subject to gravity loads from the blade, rather than in an unstressed state. Therefore, the bridges can be rebalanced (i.e., zeroed) after the fact to any desired reference condition. The most convenient reference condition is the mean strain during a slow roll at constant pitch, which occurs during the first 30 s of this dataset. Using the NREL EtherCAT data acquisition system[1] (EDAS) and for National Instruments quarter-bridge type 1 convention[2] with negligible lead-wire resistance, the strain, ε, is:

$$\varepsilon = \frac{1}{G_F} V_{\text{EDAS}} \tag{1}$$

Where the voltage ratio recorded by EDAS, V_{EDAS}, in units of V/V is

$$V_{\text{EDAS}} = \frac{-4V_r}{1+2V_r} \tag{2}$$

The result is the change in strain from the mean of the reference slow roll loading condition and at the constant temperature of 19°C. Figure 12 shows the strain for the example dataset. During the slow roll, the dynamic strain is approximately ±35 με, increasing in frequency as the rotor speed increases. When the turbine begins to generate power and thrust just after 180 s, there is also a step change in each of the responses with strains reaching 100 to 150 με.

[1] See EtherCAT DAS Software User's Manual
[2] See https://www.ni.com/docs/en-US/bundle/labview-wireless-sensor-network-module/page/niwsnhelp/quarter1.html for additional information

This report is available at no cost from the National Renewable Energy Laboratory at www.nrel.gov/publications.

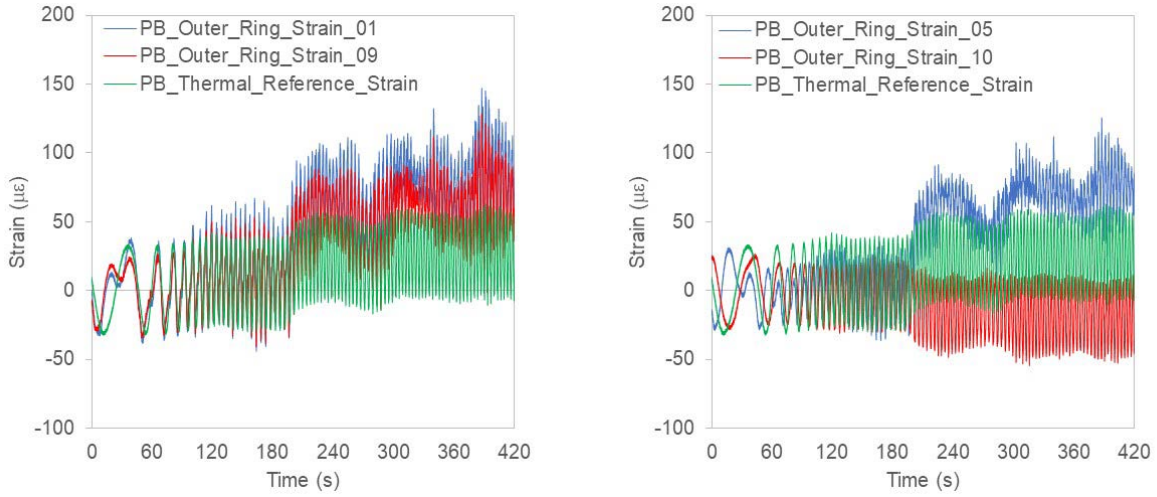

Figure 12. Outer ring trailing edge (left) and leading edge (right) strain in με over time

The correlations between strain, active power, and rotor speed for two of the strain gages are further examined in Figure 13. From the figure, it can be observed that the mean value of the strain tracks closely with changes in both the active power and rotor speed because of the increasing integrated aerodynamic and centrifugal loads. For the two strain gages shown in Figure 13, the mean strain reaches approximately 75 με above the mean of the reference slow roll condition, whereas the dynamic strains are approximately ±35 to ±60 με from the mean.

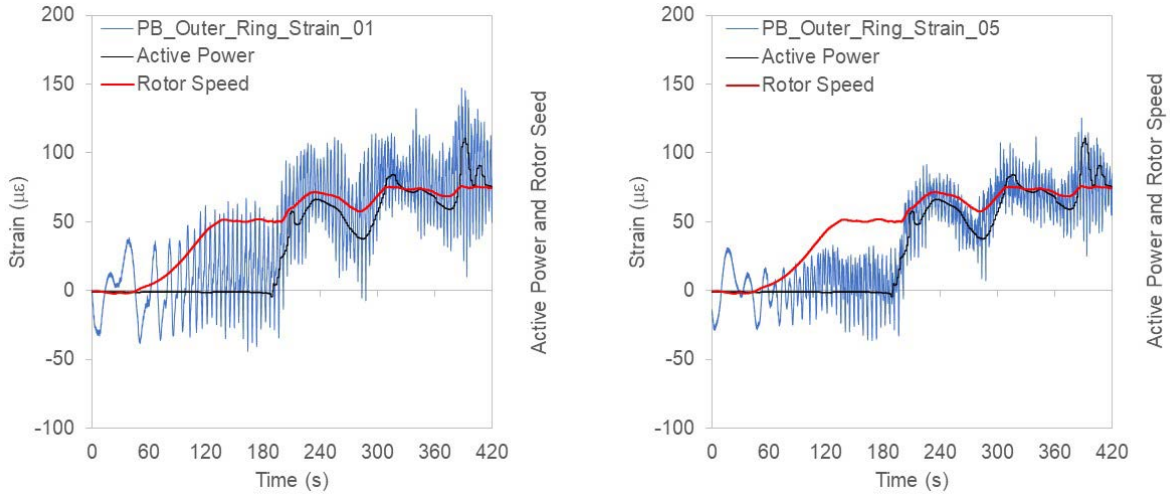

Figure 13. Outer ring trailing edge (left) and leading edge (right) strain in με compared to active power

The strain responses over the last three revolutions (10 seconds) of the rotor in this example, in which it was at near constant rotor speed and active power, are plotted in Figure 14. Each of these signals is primarily driven by the once-per-revolution loads that the pitch bearing supports, much of it from the weight and weight moment of the blade, whereas the mean strain changes with integrated aerodynamic and centrifugal loads as noted in Figure 13.

This report is available at no cost from the National Renewable Energy Laboratory at www.nrel.gov/publications.

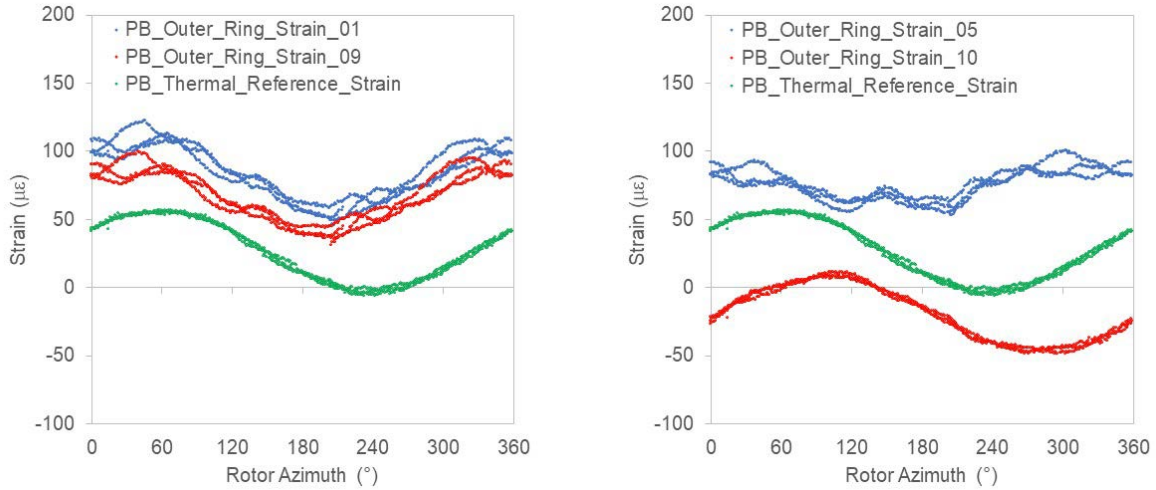

Figure 14. Outer ring trailing edge (left) and leading edge (right) strain over rotor azimuth

It should be noted that the measured bridge responses will change with temperature and must be accounted for when examining the mean strain. This temperature effect can most easily be accounted for by regularly rebalancing the strain gages during slow roll conditions over time as the temperature changes. However, if there is a relatively large change in temperature as the wind turbine operates continuously during longer periods of time (e.g., minutes to hours), the change in mean strain with temperature should also be accounted for using the thermal output coefficients for the chosen CEA-type strain gages. The effect is minimal for temperatures near and above ambient (reaching +13 με at 40°C); however, it becomes much larger as the temperature becomes colder (over -200 με at -20°C). Regardless, the very short duration dynamic strain measurements taken over an individual or a few rotor revolutions are unlikely to be affected and are easily separable from the changes in mean strain (Vishay 2007).

This effect is demonstrated in a slow roll that occurred during the morning of October 30, 2023, at 11:30 a.m. Ambient air temperatures had fallen significantly, resulting in measured temperatures on the pitch bearing inner ring and hub casting of -1°C. Figure 15 compares the measured thermal reference strain on the hub casting for this "cold" slow roll to the same "warm" slow roll at 19°C previously shown in Figure 12. The change in temperature has resulted in a shift of approximately -29 με in the mean strain, similar (but somewhat more than) to the amount projected by the thermal output coefficients for the chosen CEA-type strain gages listed in Table 3. However, the dynamic strain during the slow roll is almost identical at ±135 με. This change in the mean strain can easily be accounted for by rebalancing at -1°C, or by compensating using the thermal output coefficients (Vishay 2007).

This report is available at no cost from the National Renewable Energy Laboratory at www.nrel.gov/publications.

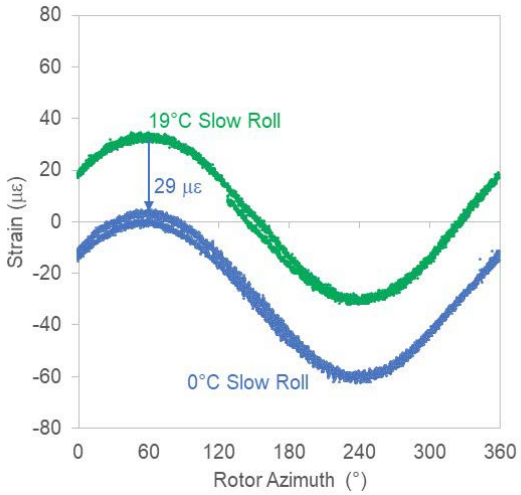

Figure 15. Effect of temperature on mean strain during a slow roll

3.2 Displacement

The relative axial displacement between the IR and OR for all four sensors are examined in Figure 16 along with the blade pitch angle. The axial displacement measurements are primarily near the midpoint of their measurement range at 25 mm. However, as the blade pitches, the effect of the passage of the pitch gear teeth can be clearly observed. Spurious readings of either 20 or 30 mm can be recorded, the clearest example of which can be seen when the blade is at a pitch angle of -1° for a prolonged period and all four sensors read a spurious displacement of 20 mm. Additionally, by plotting the sensor response against the blade pitch it becomes clear that other spurious readings between the midrange of 25 mm and the extremes result when the displacement sensor passes each tooth. This pattern occurs over the full range of blade pitch every other 1.25°. That is, valid displacement measurements occur from a blade pitch of 10° to 11.25°, spurious displacement measurements from a blade pitch of 11.25° to 12.5°, valid displacement measurements from a blade pitch of 12.5° to 13.75°, spurious displacement measurements from a blade pitch 13.75° to 15°, and so on.

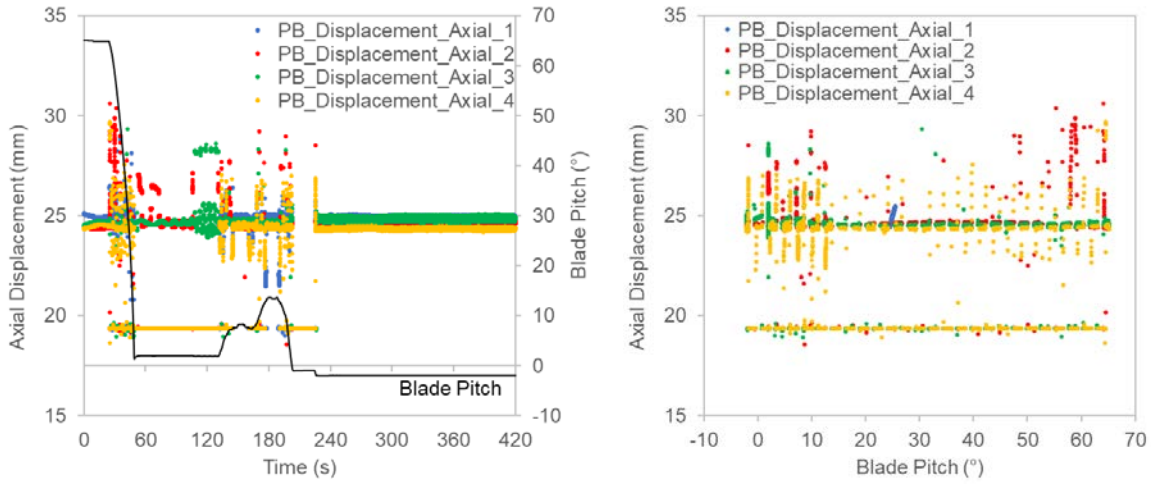

Figure 16. Relative axial displacements over time (left) and over blade pitch (right)

This report is available at no cost from the National Renewable Energy Laboratory at www.nrel.gov/publications.

Figure 17 further examines the relative axial displacements over the last three revolutions of the rotor in this example. During this period, the blade pitch was constant at -2°. Like the strain responses, the relative axial displacements are driven by the once-per-revolution loads that the pitch bearing supports. The peak-to-peak displacement is largest at 0.4 mm for sensor 2 and smallest at 0.2 mm for sensor 4.

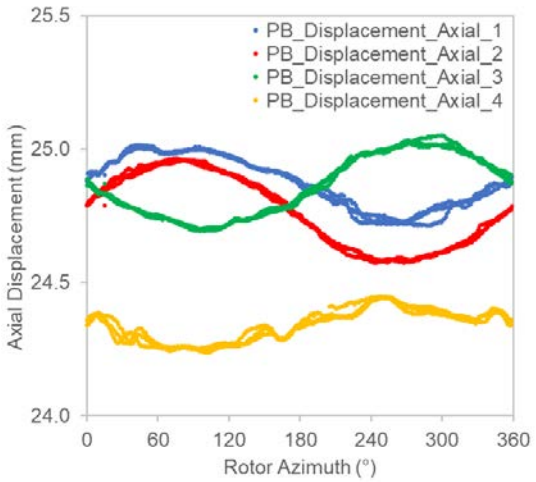

Figure 17. Relative axial displacements over rotor azimuth

This report is available at no cost from the National Renewable Energy Laboratory at www.nrel.gov/publications.

4 Conclusions

NREL has recently begun a research program related to pitch bearing reliability, recognizing its growing importance as land-based wind turbines continue to age and larger, offshore wind turbines are deployed. In this report, we describe a set of instrumentation recently installed on the DOE 1.5 turbine at NREL's Flatirons Campus and initial measurements. Additional measurements will be recorded as the wind turbine operates during late 2023 and early 2024. These measurements will be used to validate finite-element analyses of the pitch bearing.

This report is available at no cost from the National Renewable Energy Laboratory at www.nrel.gov/publications.

References

Bartschat, A., K. Behnke, and M. Stammler. 2023. "The effect of site-specific wind conditions and individual pitch control on wear of blade bearings." *Wind Energy Science* 8(10): 1495–1510. doi: 10.5194/wes-8-289-2023.

Bayles, C. 2020. "Extending wind turbine life with pitch bearing upgrades." *Windpower Engineering & Development* 12(1): 16–20. https://www.windpowerengineering.com/extending-wind-turbine-life-with-pitch-bearing-upgrades/.

Becker, D., A. Gockel, T. Handreck, B. Lüneburg, T. Netz, and G. Volmer. 2017. "State-of-the-art Design Process for Pitch Bearing Applications of Multi-MW Wind Turbine Generators." Presented at Conference for Wind Power Drives 2017.

Becker, D., J. Rollman, T. Handreck, M. Neidnicht, P. Müller, and G. Volmer. 2023. "Multi-MW Blade Bearing Applications: Advanced Bearing Calculation Process and Product Development Trends." Presented at Conference for Wind Power Drives 2023.

Behnke, K. and F. Schleich. 2023. "Exploring limiting factors of wear in pitch bearings of wind turbines with real-scale tests." *Wind Energy Science* 8(2): 289–301. doi: 10.5194/wes-8-289-2023.

Dao, C., B. Kazemtabrizi, and C. Crabtree. 2019. "Wind turbine reliability data review and impacts on levelised cost of energy." *Wind Energy* 22(12): 1848–1871. doi: 10.1002/we.2404.

Doll, G. L. 2022. "Surface engineering in wind turbine tribology." *Surface and Coatings Technology*, 442: 128545. doi: 10.1016/j.surfcoat.2022.128545.

Dhanola, A. and H. C. Garg. 2020. "Tribological challenges and advancements in wind turbine bearings: A review." *Engineering Failure Analysis* 118: 104885. doi: 10.1016/j.engfailanal.2020.104885.

Dvorak, P. 2016. "Making short lived pitch bearing work longer." *Windpower Engineering & Development*. https://www.windpowerengineering.com/making-short-lived-pitch-bearing-work-longer/.

Fischer, J. and P. Mönnig. 2019. "Challenges for the Design Process of Pitch Bearings and the Contribution of Test Benches." Presented at Conference for Wind Power Drives 2019.

Graßmann, M., F. Schleich, and M. Stammler. 2023. "Validation of a finite-element model of a wind turbine blade bearing." *Finite Elements in Analysis and Design* 221: 103957. doi: 10.1016/j.finel.2023.103957.

Grebe, M., J. Molter, F. Schwack, and G. Poll. 2018. "Damage mechanisms in pivoting rolling bearings and their differentiation and simulation." *Bearing World Journal* 3: 71–86. http://kth.diva-portal.org/smash/record.jsf?pid=diva2%3A1433594&dswid=6752.

This report is available at no cost from the National Renewable Energy Laboratory at www.nrel.gov/publications.

Handreck, T., D. Becker, J. Rollmann, B. Lüneburg. 2015. "Determining the Characteristics of Large Diameter Ball and Roller Bearings." Presented at Conference for Wind Power Drives 2015.

Harris, T., J. H. Rumbarger, and C. P. Butterfield. 2009. *Wind Turbine Design Guideline DG03: Yaw and Pitch Rolling Bearing Life*. Golden, CO: National Renewable Energy Laboratory (NREL). NREL/TP-500-42362. https://www.nrel.gov/docs/fy10osti/42362.pdf.

He, P., R. Hong, H. Wang, and C. Lu. 2018. "Fatigue life analysis of slewing bearings in wind turbines." *International Journal of Fatigue* 111: 233–242. doi: 10.1016/j.ijfatigue.2018.02.024.

Hornemann, M. 2019. "Top failure observations from the field." Presented at Drivetrain Reliability Collaborative Meeting, February 20, 2019. https://app.box.com/s/7vo2ssy085raoeqa8wnyh5lrfjne6lgs.

Kaydon. n.d. "Kaydon slewing bearings." https://www.kaydonbearings.com/DT_turntable_bearings.htm.

Keller, J. and Y. Guo. 2022. *Rating of a Pitch Bearing for a 1.5-Megawatt Wind Turbine.* Golden, CO: National Renewable Energy Laboratory (NREL). NREL/TP-5000-82462. https://www.nrel.gov/docs/fy23osti/82462.pdf.

Keller, J., S. Sheng, Y. Guo, B. Gould, and A. Greco. 2021. *Wind Turbine Drivetrain Reliability and Wind Plant Operations and Maintenance Research and Development Opportunities*. Golden, CO: National Renewable Energy Laboratory (NREL). NREL/TP-5000-80195. https://www.nrel.gov/docs/fy21osti/80195.pdf.

Liu, R., H. Wang, B. T. Pang, X. H. Gao, and H. Y. Zong. 2018. "Load Distribution Calculation of a four-Point-Contact Slewing Bearing and its Experimental Verification." *Experimental Techniques* 42: 243–252. doi: 10.1007/s40799-018-0237-2.

de la Presilla, R., S. Wandel, M. Stammler, M. Grebe, G. Poll, and S. Glavatskih. 2023. "Oscillating rolling element bearings: A review of tribotesting and analysis approaches." *Tribology International* 188: 108805. doi: 10.1016/j.triboint.2023.108805.

Santos, R. and J. van Dam. 2015. *Mechanical Loads Test Report for the U.S. Department of Energy 1.5-Megawatt Wind Turbine*. Golden, CO: National Renewable Energy Laboratory (NREL). NREL/TP-5000-63679. http://www.nrel.gov/docs/fy15osti/63679.pdf.

Schwack, F., F. Prigge, and G. Poll. 2018. "Finite element simulation and experimental analysis of false brinelling and fretting corrosion." *Tribology International* 126: 352–362. doi: 10.1016/j.triboint.2018.05.013.

Schwack, F., N. Bader, J. Leckner, C. Demaille, and G. Poll. 2020. "A study of grease lubricants under wind turbine pitch bearing conditions." *Wear* 454–455: 203335. doi: 10.1016/j.wear.2020.203335.

This report is available at no cost from the National Renewable Energy Laboratory at www.nrel.gov/publications.

Schwack, F., F. Halmos, M. Stammler, G. Poll, S. Glavatskih. 2021. "Wear in wind turbine pitch bearings—A comparative design study." *Wind Energy* 25(4): 700–718. doi: 10.1002/we.2693.

Shapiro, J. 2017. "Pitch Bearing Investigations." Presented at Drivetrain Reliability Collaborative Meeting, February 21, 2017. https://app.box.com/s/tgv9r5vpwslex2f4uh5ssk1qtwev0bxq.

Song, W. and A. K. Karikari-Boateng. 2021. "Enhanced Test Strategy of Pitch Bearing Based on Detailed Motion Profile." Presented at Conference for Wind Power Drives 2021.

Stehly, T., P. Beiter, and P. Duffy. 2020. *2019 Cost of Wind Energy Review*. Golden, CO: National Renewable Energy Laboratory (NREL). NREL/TP-5000-78471. https://www.nrel.gov/docs/fy21osti/78471.pdf.

Vishay Micro-Measurements. 2007. *Strain Gage Thermal Output and Gage Factor Variation with Temperature*. Tech Note TN-504-1. https://docs.micro-measurements.com/?id=2405.

Walgern, J., K. Fischer, P. Hentschel, and A. Kolios. 2023. "Reliability of electrical and hydraulic pitch systems in wind turbines based on field-data analysis." *Energy Reports* 9: 3273–3281. doi: 10.1016/j.egyr.2023.02.007.

Wiser, R., M. Bolinger, and E. Lantz. 2019. "Assessing wind power operating costs in the United States: Results from a survey of wind industry experts." *Renewable Energy Focus* 30: 46–57. doi: 10.1016/j.ref.2019.05.003.

Wiser, R., M. Bolinger, B. Hoen, D. Millstein, J. Rand, G. Barbose, N. Darghouth, W. Gorman, S. Jeong, E. O'Shaughnessy, and B. Paulos. 2023. *Land-Based Wind Market Report: 2023 Edition*. doi: 10.2172/1996790.

This report is available at no cost from the National Renewable Energy Laboratory at www.nrel.gov/publications.

Appendix A. Pitch Bearing Instrumentation Details

Figure A-1 shows the location of the strain gauges on the pitch bearing outer ring and inner ring.

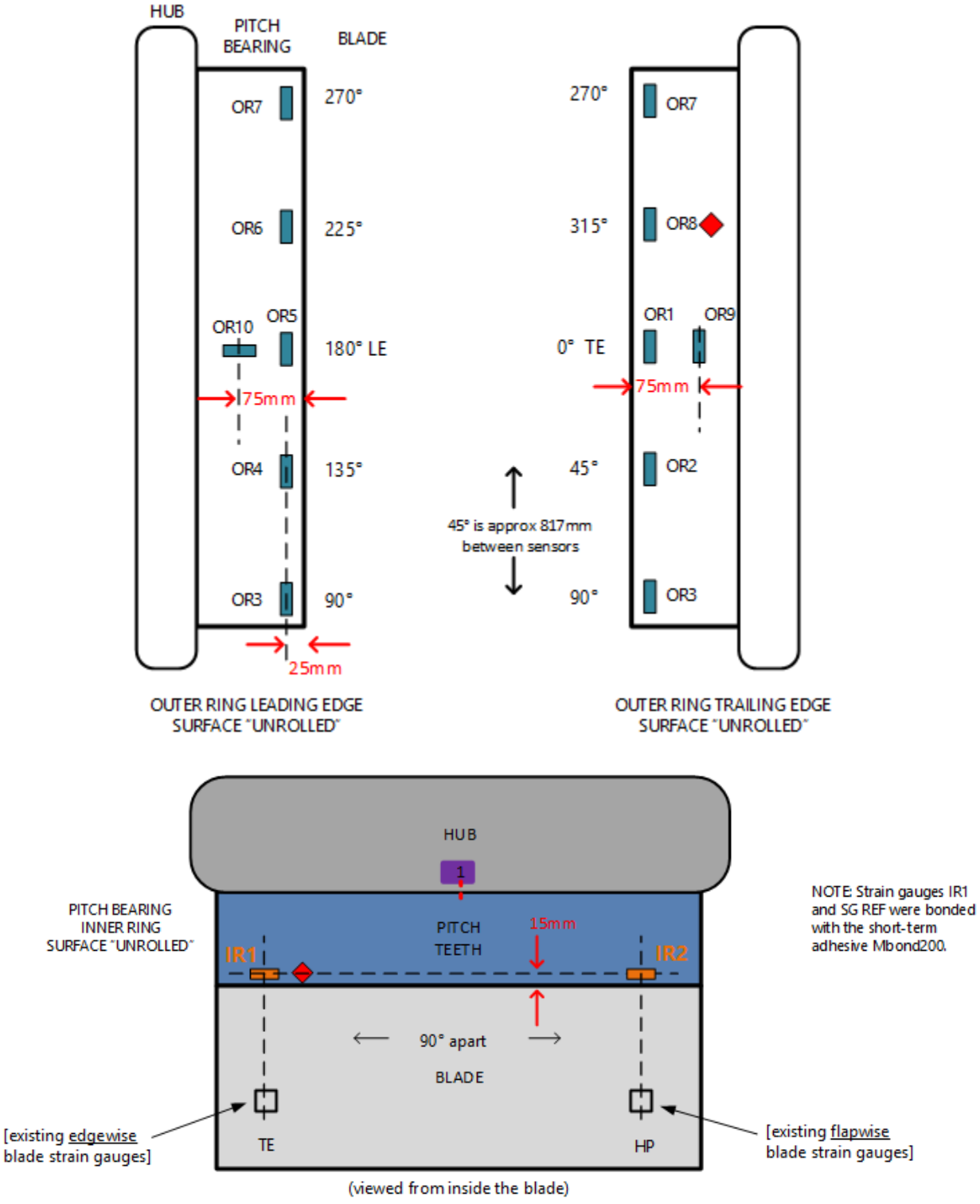

Figure A-1. Pitch bearing strain gage locations

This report is available at no cost from the National Renewable Energy Laboratory at www.nrel.gov/publications.

Table A-1 summarizes the pitch bearing instrumentation package.

Table A-1. Pitch Bearing Instrumentation Details

Channel	Units	Location	Orientation	Sensor	Note
PB_Outer_Ring_Strain_01	volts per unit volt (V/V)	Outer ring at 0°	Circumferential	CEA-06-250UWA-350	
PB_Outer_Ring_Strain_02	V/V	Outer ring at 45°	Circumferential	CEA-06-250UWA-350	
PB_Outer_Ring_Strain_03	V/V	Outer ring at 90°	Circumferential	CEA-06-250UWA-350	
PB_Outer_Ring_Strain_04	V/V	Outer ring at 135°	Circumferential	CEA-06-250UWA-350	Connected to National Instruments quarter-bridge 9236 card
PB_Outer_Ring_Strain_05	V/V	Outer ring at 180°	Circumferential	CEA-06-250UWA-350	
PB_Outer_Ring_Strain_06	V/V	Outer ring at 225°	Circumferential	CEA-06-250UWA-350	
PB_Outer_Ring_Strain_07	V/V	Outer ring at 270°	Circumferential	CEA-06-250UWA-350	
PB_Outer_Ring_Strain_08	V/V	Outer ring at 315°	Circumferential	CEA-06-250UWA-350	
PB_Outer_Ring_Strain_09	V/V	Outer ring at 0° (hub side)	Circumferential	CEA-06-250UWA-350	
PB_Outer_Ring_Strain_10	V/V	Outer ring at 180° (hub side)	Axial	CEA-06-250UWA-350	
PB_Inner_Ring_Strain_01	V/V	Inner ring at trailing edge	Circumferential	CEA-06-250UWA-350	Connected to National Instruments quarter-bridge 9236 card
PB_Inner_Ring_Strain_02	V/V	Inner ring on upwind side	Circumferential	CEA-06-250UWA-350	
PB_Thermal_Reference_Strain	V/V	Hub casting interior	-	CEA-06-250UWA-350	

This report is available at no cost from the National Renewable Energy Laboratory at www.nrel.gov/publications.

Channel	Units	Location	Orientation	Sensor	Note
PB_Displacement_Axial_1	millimeters (mm)	Inner ring teeth	Axial	optoNCDT ILD1220-10	
PB_Displacement_Axial_2	mm	Inner ring teeth	Axial	optoNCDT ILD1220-10	Connected to 500 Ω resistor and National Instruments voltage input 9239 card
PB_Displacement_Axial_3	mm	Inner ring teeth	Axial	optoNCDT ILD1220-10	
PB_Displacement_Axial_4	mm	Inner ring teeth	Axial	optoNCDT ILD1220-10	
PB_Surface_Temperature_OR	degrees Celsius (°C)	Outer ring	-	SSP-RTD-PT100-180-MP	Connected to DAT 4531B resistance temperature detector converter, 500 Ω resistor, and National Instruments voltage input 9239 card
PB_Surface_Temperature_IR	°C	Inner ring	-	SSP-RTD-PT100-180-MP	
PB_Thermal_Reference_Temp	°C	Hub casting interior	-	SSP-RTD-PT100-180-MP	

This report is available at no cost from the National Renewable Energy Laboratory at www.nrel.gov/publications.